ELSEVIER

Journal of Alloys and Compounds 356–357 (2003) 114–119

Journal of ALLOYS AND COMPOUNDS

www.elsevier.com/locate/jallcom

Structure stability maps for intermetallic AB_5 compounds

L. Guénée, K. Yvon*

Laboratoire de Cristallographie, Université de Genève, 24 Quai Ernest-Ansermet, CH-1211 Geneva 4, Switzerland

Received 26 August 2002; accepted 1 September 2002

Abstract

The structural stability of AB_5 compounds (A=lanthanide, alkaline earth, transition element; B=d- and/or p-block element) has been modelled in terms of atomic properties and represented in the form of structure stability maps. The results on some 520 known binary and ternary known representatives show that the various structure types form rather well-defined stability domains in three-dimensional space spanned by valence electron concentration, VEC, electronegativity difference, $\Delta\chi$, and radius ratio, R_A/R_B. Emphasis is placed on hexagonal $CaCu_5$ type compounds that occur within the intervals $5.5<VEC<9.5$, $-0.3<\Delta\chi<0.1$ and $1.3<R_A/R_B<1.5$. The maps are of interest for the search of new hydrogen storage materials, in particular those containing light and inexpensive 3d transition metals (Fe, Mn, etc.).

Keywords: Intermetallic compounds; Crystal structure; Valence electron concentration; Atom size; Electronegativity; Metal hydrides

1. Introduction

Intermetallic compounds of composition AB_5 (A=lanthanide, alkaline earth, transition element; B=d- and/or p-block element), in particular those crystallizing with the hexagonal $CaCu_5$ type structure and their ternary derivatives, are of interest for various technological applications such as permanent magnets and hydrogen storage. They crystallize with at least 20 different structure types. In order to find new AB_5 compounds it was of interest to model their structural stability in terms of atomic properties. Modeling of various structures based on purely geometrical grounds has been made some time ago by dimensional analysis of measured cell parameters, interatomic distances and tabulated sets of atomic radii (see, for example, Ref. [1]). Recently, the stability regime of the $CaCu_5$ structure has been re-investigated by this method for some 50 known binary representatives containing rare-earth (R) and transition elements [2]. The analysis was based on measured structure parameters which means that its predictive power could not be easily tested. In this work, an analysis is made based on atomic properties along the lines of Ref. [3] and others. Both binary and ternary compositions are included, covering a total of 520 compounds that crystallize with some 15 structure types. It will be shown that the various structures occupy well defined stability domains in three-dimensional space spanned by valence electron concentration (VEC), electronegativity difference ($\Delta\chi$) and radius ratio (R_A/R_B). The predictive power of the analysis was tested on a few examples. Special attention was payed to $CaCu_5$ type compounds because of their importance in the energy sector.

2. Model

The structural stability of binary AB_5 and ternary $A(B,B')_5$ compounds (A=rare earth, alkaline earth, Zr, Hf, Th; B=transition elements and/or p-block element such as Al, Ga, Sn, In, Si, Ge) was modelled in terms of three parameters:

2.1. Geometric factor

The influence of atomic size was described by the radius ratio R_A/R_B as calculated from a tabulated set of atom radii [4]. For ternary compositions $AB_{5-x}B'_x$ an average radius for the B component was calculated according to the relation $R_{BB'}=[(5-x)R_B+xR_{B'}]/5$.

*Corresponding author. Tel.: +41-22-702-6231; fax: +41-22-702-6864.

E-mail address: klaus.yvon@cryst.unige.ch (K. Yvon).

0925-8388/03/$ – see front matter
doi:10.1016/S0925-8388(03)00167-1

2.2. Electronegativity

Its influence was described by the electronegativity difference $\Delta\chi = 2/6[\chi_A - \chi_B]$ as calculated from values reported by [5]. For ternary compositions $AB_{5-x}B'_x$ an average value for the B component was calculated according to the relation $\chi_{BB'} = [(5-x)\chi_B + x\chi_{B'}]/5$.

2.3. Valence electron concentration (VEC)

For binary AB_5 compounds its value was calculated as $VEC = (VE_A + 5VE_B)/6$ and for ternary $AB_{5-x}B'_x$ compounds as $VEC = (VE_A + (5-x)VE_B + xVE_{B'})/6$ (VE_A, VE_B, number of valence electrons of A and B atoms). Full valences were used, such as VE(Cu)=11, VE(Th)=4, VE(*R*)=3 (except for Ce^{IV}, Eu^{II} and Yb^{II}).

2.4. Structure data

The compositions and structures of AB_5 compounds were retrieved from the following sources: *Pearson's Handbook of Crystallographic Data for Intermetallic Phases* [6], *Atlas of Crystal Structure Types for Intermetallic Phases* [7], *Binary Alloy Phase Diagrams* [8], *Handbook of Ternary Alloy Phase Diagrams* [9], and *Red Books* [10]. The structure types covered, and their symmetry and number of representatives are summarised in Table 1. Those containing boron and silicon are included in the maps but not discussed in detail because of their specific crystal chemistry. On the other hand, structure types having few representatives such as $LuMn_5$, $ErZn_5$, $MgZn_5$, $MnCu_4In$, $LaAl_4Co$, YAl_4Ni, $ScNi_2Si_3$ and $LiMg_2Zn_3$ are not included in Table 1. For each compound appropriate values for R_A/R_B, $\Delta\chi$ and VEC were calculated (for a detailed list see Ref. [11]) and used to construct structural stability maps (called 'maps' thereafter). For clearness, the maps of binary and ternary compounds are presented separately. That for the binary compounds was drawn as a function of R_A/R_B and $\Delta\chi$ for various VEC as shown in Fig. 1, whereas those for the ternary compounds were drawn in VEC intervals of $9 \le VEC < 10$, $8 \le VEC < 9$, $7 \le VEC < 8$, $6 \le VEC < 7$ and $5 \le VEC < 6$ as shown in Figs. 2–6, respectively. The compounds in these maps appear as data points with appropriate symbols that refer to the various structure types.

Table 1
Structure types, space groups, VEC ranges and number of representatives

Structure type	Space group	VEC range	Number of representatives	Figure
$CaCu_5$	*P6/mmm*	5–10	194	1–6
$AuBe_5$ ($MgCu_4Sn$[c])	*F43m*	3–10	74	1–4
$PrNi_2Al_3$[a]	*P6/mmm*	5–6	10	6
YNi_2Al_3[b]	*P6/mmm*	5–7	50	5,6
$SmAg_{3.5}Al_{1.5}$[g]	*P 62m*	7–8	3	4
$BaZn_5$	*Cmcm*	5–6	6	6
$DyAg_{2.4}Al_{2.6}$[f]	*P6$_3$/mmc*	6–7	10	5
$Nd_3Ni_{13}B_2$[d]	*P6/mmm*	9–10	12	2
$CeCo_4B$[d]	*P6/mmm*	5–8	30	4–6
$CeCo_3B_2$[a]	*P6/mmm*	5–7	32	5,6
$LaRu_3Si_2$[e]	*P6$_3$/m*	5–6	3	6
$ErRh_3Si_2$[e]	*Imma*	6–7	9	5
$ErIr_3B_2$[e]	*C2/m*	6–7	20	5
$Ce_2Co_7B_3$[d]	*P6/mmm*	6–7	11	5
$Ce_3Co_{11}B_4$[d]	*P6/mmm*	8–9	12	3

[a] Ordered derivative of $CaCu_5$.
[b] Stacking block variant of $CaCu_5$ with cell parameter relationships $a = a_{CaCu5}\sqrt{3}$ and $c = c_{CaCu5}$, also called $HoNi_{2.6}Ga_{2.4}$ type.
[c] Ordered substitution derivative of $AuBe_5$.
[d] Stacking variant of $CaCu_5$ and YNi_2Al_3.
[e] Distorted (low-symmetry) variant of $CeCo_3B_2$.
[f] Disordered derivative of $ErZn_5$.
[g] Disordered derivative of $CaCu_5$.

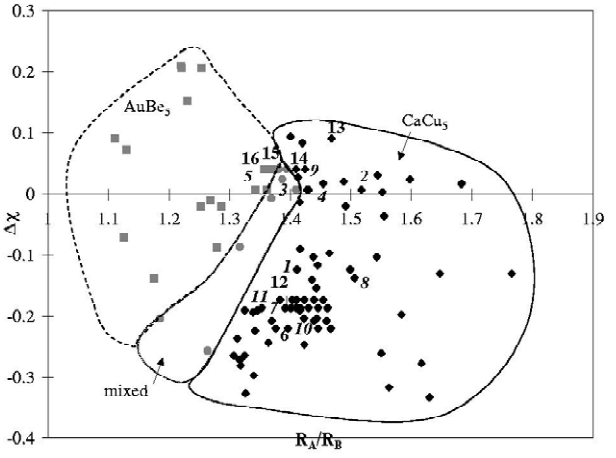

Fig. 1. Structure stability map for binary AB_5 compounds. (**1**) $ThFe_5$, (**2**) $Yb(2)Cu_5$, (**3**) $Yb(3)Cu_5$, (**4**) $Ce(3)Cu_5$, (**5**) $Ce(4)Cu_5$, (**6**) $CeNi_5$, (**7**) $CeCo_5$, (**8**) $LaNi_5$, (**9**) $NdCu_5$, (**10**) $DyNi_5$, (**11**) $Ce^{IV}Fe_5$, (**12**) $LuNi_5$, (**13**) $LaCu_5$, (**14**) $SmCu_5$, (**15**) $ErCu_5$, (**16**) $LuCu_5$.

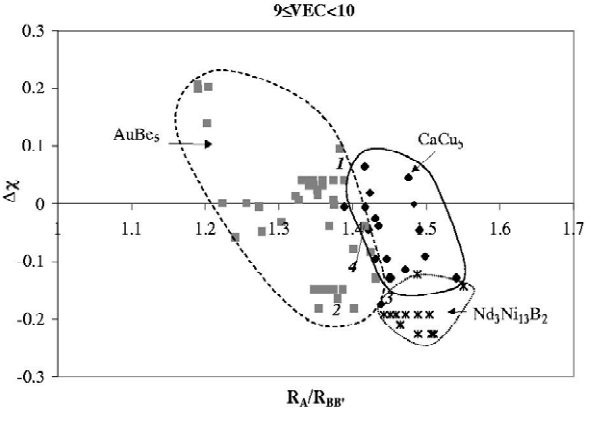

Fig. 2. Structure stability map for ternary $AB_{5-x}B'_x$ compounds with $9 \le VEC < 10$. (**1**) $NdCu_4Ag$, (**2**) $DyNi_4Au$, (**3**) $GdNi_4Cu$, (**4**) $GdCu_4Ni$.

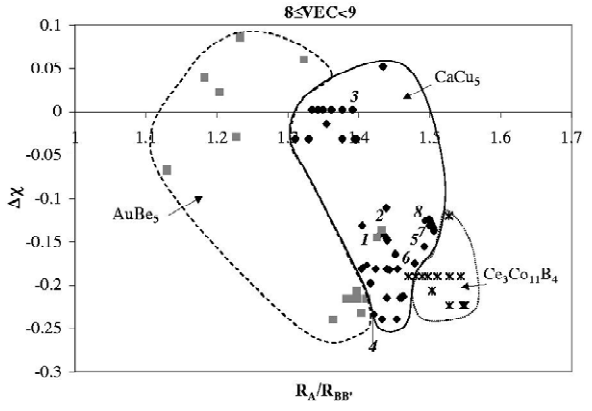

Fig. 3. Structure stability map for ternary $AB_{5-x}B'_x$ compounds with 8≤VEC<9. (**1**) $YNi_{3.5}Mn_{1.5}$, (**2**) YNi_4Mn, (**3**) $NdCu_4Al$, (**4**) $CeNi_{4.3}Mn_{0.7}$, (**5**) $LaNi_4Mn$, (**6**) $LaNi_3Mn_2$, (**7**) $LaNi_4Fe$, (**8**) $LaNi_3Fe_2$.

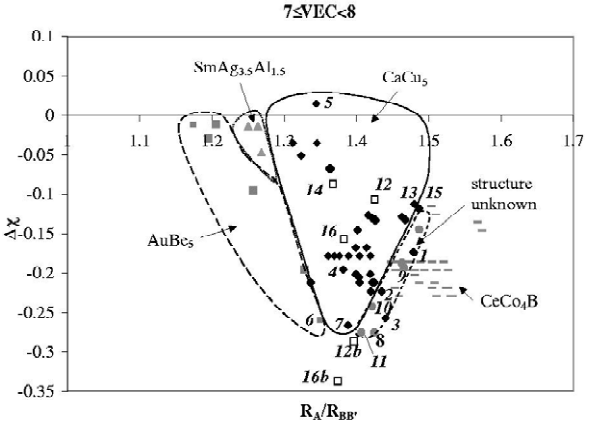

Fig. 4. Structure stability map for ternary $AB_{5-x}B'_x$ compounds with 7≤VEC<8. (**1**) $LaNi_3Mn_2$, (**2**) $NdNi_3Mn_2$, (**3**) $PrNi_3Mn_2$, (**4**) $DyNi_4Al$, (**5**) YCu_3Al_2, (**6**) $CeNi_3Mn_2$, (**7**) $CeNi_{2.5}Mn_{2.5}$, (**8**) $CeNi_2Mn_3$, (**9**) $LaNi_2Mn_3$, (**10**) $NdNi_2Mn_3$, (**11**) $GdNi_2Mn_3$, (**12**) $LaNi_4Mg$, (**12b**) $(La_{0.5}Mg_{0.5})Ni_2$, (**13**) $LaFe_4Ni$, (**14**) YNi_4Mg, (**15**) $LaNi_2Fe_3$, (**16**) $NdNi_4Mg$, (**16b**) $(La_{0.5}Mg_{0.5})Ni_2$.

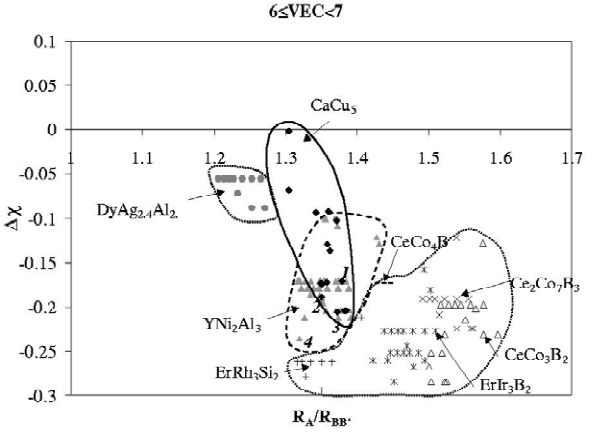

Fig. 5. Structure stability map for ternary $AB_{5-x}B'_x$ compounds with 6≤VEC<7. (**1**) $NdNi_3Al_2$, (**2**) $DyNi_3Ga_2$, (**3**) $GdNi_3Ga_2$, (**4**) $GdNi_3Sn_2$.

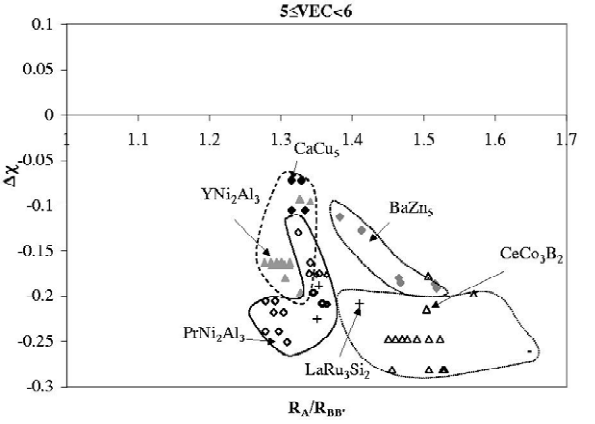

Fig. 6. Structure stability map for ternary $AB_{5-x}B'_x$ compounds with 5≤VEC<6.

3. Results

3.1. Domains of stability

As expected AB_5 compounds crystallising with the same structure are concentrated in the maps in domains of structural stability (called 'domains' hereafter). The domains are relatively well defined for commonly occurring structure types such as $CaCu_5$ (194 members), $AuBe_5$ (74) and YNi_2Al_3 (50) (see closed lines in Figs. 1–6) but less well defined for uncommon structure types such as $LaRu_3Si_2$ (3) that overlaps with the structurally related $CeCo_3B_3$ (32) and $ErRh_3Si_2$ (9) domains (see Figs. 5 and 6), and $PrNi_2Al_3$ (10) that overlaps with YNi_2Al_3 (Fig. 6). As expected, some overlap also exists between the structurally related YNi_2Al_3, $CaCu_5$ and $CeCo_4B$ (30) domains (Figs. 4 and 5), and the $CaCu_5$ domain is not well defined for low VEC values for which it overlaps with the YNi_2Al_3 and $PrNi_2Al_3$ domains (Figs. 5 and 6). For binary compositions AB_5 the major domains are $CaCu_5$ and $AuBe_5$ type (Fig. 1). Both extend over relatively wide VEC intervals ($CaCu_5$: 7.3<VEC<10.3; $AuBe_5$: 3<VEC<9.8, VEC values not indicated in Fig. 1 but listed in Ref. [11]) which suggests that electron concentration is not of major importance for structural stability. On the other hand, the geometric factor appears to be important because big radii ratios favour $CaCu_5$ type (R_A/R_B>1.4) and small ratios $AuBe_5$ type structures (R_A/R_B<1.3). For intermediate ratios the domains overlap (see 'mixed' region in Fig. 1). This is due to the fact that $AuBe_5$ type structures tend to form at low and $CaCu_5$-type structures at high temperature. Electronegativity appears to be less important for structural stability because the $\Delta\chi$ ranges are relatively wide and do not much differ between structure types ($CaCu_5$: $-0.3<\Delta\chi<0.1$; $AuBe_5$: $-0.2<\Delta\chi<0.2$).

For ternary compositions $AB_{5-x}B'_x$ (Figs. 2–6) at least 15 (for complete list see Ref. [11]) different structure

domains occur of which the $CaCu_5$ type is the most important. Compared to the binary compounds the latter extends over a wider VEC range (5.5<VEC<9.5) and towards lower VEC values (see for example $NdNi_3Al_2$; VEC=6.5, (**1**) in Fig. 5). Yet valence appears to play an important role because the domain size and shape changes considerably as a function of VEC. As VEC decreases the number of different structure types generally increases. At high VEC (8<VEC<10) four domains appear ($CaCu_5$, $AuBe_5$, $Nd_3Ni_{13}B_2$, $Ce_3Co_{11}B_4$) while at low VEC seven (5<VEC<6) and eight (6<VEC<7) domains appear. At high VEC values (9≤VEC<10) $AuBe_5$ type structures prevail while at low values (5≤VEC<6) $PrNi_2Al_3$, $CeCo_3B_2$ and YNi_2Al_3 type structures prevail. VEC values below 7 appear to preclude the formation of $AuBe_5$ type structures and values below 8 preclude $Nd_3Ni_{13}B_2$ and $Ce_3Co_{11}B_4$ type structures. As to the geometric factor low $R_A/R_{BB'}$ values favour the $AuBe_5$ type ($1.1<R_A/R_{BB}<1.3$) and high values the $CaCu_5$ type ($1.3<R_A/R_{BB}<1.5$). The highest $R_A/R_{BB'}$ values occur with $CeCo_3B_2$, $CaRh_3B_2$, $Ce_2Co_7B_3$ and $CeCo_4B$ type structures ($1.5<R_A/R_{BB}<1.6$). Electronegativity is important because the domains limits depend strongly on $\Delta\chi$. As to the YNi_2Al_3 type structures they appear to be governed mainly by the VEC. They are situated in a relatively narrow interval of 5.5<VEC<7 and are at the border of the $CaCu_5$ domain at high and of the $PrNi_2Al_3$ domain at low VEC values. The geometric factor appears to be less important in view of the relatively wide range of $1.28<R_A/R_B<1.45$. $BaZn_5$ type structures appear only at relatively big R_A/R_B values (Fig. 6).

In summary, the model allows one to rationalize the structural stability of 480 known AB_5 and $A(B,B')_5$ compounds. Only six compounds appear to be less well situated. Among these three $CaCu_5$-type compounds (ANi_3Mn_2, A=La, Nd, Pr; VEC=7.83; see (**1**), (**2**) and (**3**) in Fig. 4) are slightly outside their domain in the 8≤VEC<9 map (they would be inside their domain in the 8≤VEC<9 map), while the two $AuBe_5$ type compounds ($YNi_{3.5}Mn_{1.5}$, YNi_4Mn; *1* and *2* in Fig. 3) and a recently reported $MgCu_4Sn$ type compound (YNi_4Mg [12], (**14**) in Fig. 4) are in the $CaCu_5$ domain (for a possible explanation see below). Thus more than 98% of the compounds is correctly reproduced by the maps. The validity of these maps can be demonstrated by the following examples.

3.2. Selected examples

3.2.1. Binary $CaCu_5$ type structures

In the presence of trivalent A components such as rare earths, B components having less than nine valence electrons (Ti, V, Cr, Mn, Fe) and more than 11 valence electrons (Zn) do not form $CaCu_5$ type structures under normal synthesis conditions because their VEC is presumably too low (VEC=7.17) and to high (VEC=10.5), respectively. However, this structure forms with tetravalent A components such as Th, as shown by $ThFe_5$ ((**1**) in Fig. 1, VEC=7.33) which is the only known iron-based member of that type. The influence of atom valence and size on the stability domain of $CaCu_5$ type structures can be seen on the maps for R elements that are not necessarily trivalent such as Ce, Yb and Eu. Ytterbium in $YbCu_5$, for example, is divalent in the (low-pressure) $CaCu_5$ type polymorph ((**2**) in Fig. 1, $R_A/R_B=1.518$) and trivalent in the high-pressure $AuBe_5$ type polymorph ((**3**) in Fig. 1, $R_A/R_B=1.362$), in agreement with literature. As to cerium, it is known to be trivalent in the $CaCu_5$ type compound $CeCu_5$ ((**4**) in Fig. 1) but higher-valent in the structural analogues $CeNi_5$ ((**6**) in Fig. 1) and $CeCo_5$ ((**7**) in Fig. 1). These findings are consistent with the maps in which $CeCu_5$ would be situated in the $AuBe_5$ domain ((**5**) in Fig. 1) if its Ce valency was >3. Yet, no such compound has been reported so far.

3.2.2. $CaCu_5$ versus $AuBe_5$ type structures

At high VEC values (8<VEC<10) the limits between $CaCu_5$ and $AuBe_5$ domains shift to higher $R_A/R_{BB'}$ values as the VEC is increased (see maps 8<VEC<9 and 9<VEC<10). Thus $AuBe_5$ type compounds are expected to be stabilised by substituting B atoms of either higher valence and similar atom size, or of similar valence and bigger atom size. This is confirmed by the solubility of Ag, Au and Al in ACu_5 and ANi_5 (A=rare earth). Substitution of Cu and Ni in $CaCu_5$ type $NdCu_5$ and $DyNi_5$ ((**9**) and (**10**) in Fig. 1) by bigger Ag and Au decreases $R_A/R_{BB'}$ and stabilises the $AuBe_5$ type compounds $NdCu_4Ag$ and $DyNi_4Au$ ((**1**) and (**2**) in Fig. 2), while substitution by lower valent Al maintains the $CaCu_5$ type structure in $NdCu_4Al$ ((**3**) in Fig. 3, VEC=8.33) and $DyNi_4Al$ ((**4**) in Fig. 4, VEC=7.67) in spite of their smaller $R_A/R_{BB'}$.

3.2.3. Solid solutions $ACo_{5-x}Ni_x$ and $ACu_{5-x}Ni_x$ (A=rare earths)

According to the maps both series are expected to crystallise with the structure types of the corresponding binary compounds ACo_5 and ANi_5 ($CaCu_5$ type, see for example (**12**)-$LuNi_5$ in Fig. 1) and ACu_5 ($CaCu_5$ type for A=La ((**13**) in Fig. 1)–Sm (**14**), $AuBe_5$ type for A=Er (**15**)–Lu (**16**), mixed for A=Gd–Ho). Literature data in fact confirm that $ACo_{5-x}Ni_x$ forms a continuous solid solution ($0\le x\le 1$) with $CaCu_5$ type structure, as does $ACu_{5-x}Ni_x$ (A=La–Sm,Y). For heavy (small) rare earths and copper-rich compositions the latter series crystallizes with $AuBe_5$ type structures ((**4**)-$GdCu_4Ni$ in Fig. 2) and for Ni-rich compositions with $CaCu_5$ type structures ((**3**)-$GdNi_4Cu$ in Fig. 2).

3.2.4. Solubility of Mn in $CeNi_5$

Literature data show that the $CeNi_{5-x}Mn_x$ series crystallizes with $CaCu_5$ type structure for $x\le 0.7$ and $2.4\le x\le 2.7$ and $AuBe_5$ type structure for $0.9\le x\le 2.1$. For $x=3$ an undetermined hexagonal structure occurs. Inspection of the

maps suggest that these structural changes are accompanied by a valence change of cerium from Ce^{IV} in Ni-rich compositions to Ce^{III} in Mn-rich compositions as shown by $CeNi_{4.3}Mn_{0.7}$ ((**4**) in Fig. 3) and $CeNi_3Mn_2$, $CeNi_{2.5}Mn_{2.5}$ and $CeNi_2Mn_3$ ((**6**), (**7**) and (**8**) in Fig. 4) that are at the limit of the $CaCu_5$ domain. A trivalent valence state of cerium in the latter is consistent with the existence of ANi_2Mn_3 analogues with trivalent A components such as R=La, Nd, Gd ((**9**), (**10**) and (**11**) in Fig. 4).

3.2.5. Solubility limits of $LaNi_{5-x}B'_x$ (B'=Mn, Al, Cu, Co, Fe)

These $CaCu_5$ type systems are of particular interest for applications as rechargeable metal hydride electrodes. For the manganese series the maps reproduce well the observed solubility limit at x=2.1 (see (**8**)-$LaNi_5$ in Fig. 1 and (**5**)-$LaNi_4Mn$ and (**6**)-$LaNi_3Mn_2$ in Fig. 3). Although $LaNi_3Mn_2$ ((**1**) in Fig. 4, VEC=7.83) is situated slightly outside the $CaCu_5$ domain on the 7≤VEC<8 map, it is inside the domain on the 8≤VEC<9 map ((**6**) in Fig. 3). At higher Mn contents the compositions $2<x\leq2.5$ (7≤VEC<8) and $4\leq x\leq5$ (6≤VEC<7) are clearly outside the $CaCu_5$ domain, in agreement with literature. For the Al series the reported limit of solid solution (x=1) is close to that suggested by the maps (x~1.5) (VEC=7.667, inside the $CaCu_5$ domain in the 7<VEC<8 map, outside in the 6≤VEC<7 map). For the Cu series the maps suggest a complete solid solution ($0\leq x\leq1$), in accordance with literature. For the Fe series the maps suggest a solubility limit of x~2 (see (**7**)-$LaNi_4Fe$, (**8**)-$LaNi_3Fe_2$ in Fig. 3), again in accordance with literature. The hypothetical compound $LaNi_2Fe_3$ is outside the $CaCu_5$ domain ((**15**) in Fig. 4) while the hypothetical compound $LaNiFe_4$ ((**13**) in Fig. 4) is close to its border.

3.2.6. $CaCu_5$ versus YNi_2Al_3 type structures

Aluminium- and gallium-rich compounds $AB_{5-x}B'_x$ with x>2.5 crystallise mainly with YNi_2Al_3 type structures. Clearly, their domain of existence superposes in part with the $CaCu_5$ domain (Figs. 5 and 6). This is due to the fact that some compounds adopt both structures, i.e., $CaCu_5$ type for as cast, and YNi_2Al_3 type for annealed conditions (see (**2**)-$DyNi_3Ga_2$ and (**3**)-$GdNi_3Ga_2$ in Fig. 5). A similar dimorphism occurs also with the recently reported $GdNi_3Sn_2$ [13] (R_A/R_B=1.320, VEC=6.833, $\Delta\chi$=−0.236, (**4**) in Fig. 5).

3.3. Attempts to synthesise new AB_5 compounds

In order to test the usefulness of the maps a few compositions were selected for which compound formation was either not reported or the structure not known. Note that the compositions selected on the maps refer to structural rather than thermodynamic stability. In order to avoid formation of 'pseudo-ternary' solid solutions only those compositions were tested that involve systems not known to form binary AB_5 compounds.

3.3.1. $CeFe_5$

Iron-based compounds AFe_5 are expected to crystallize with $CaCu_5$ type structures only if the A component is tetravalent. According to the maps Ce^{IV} would be a candidate capable of stabilising that structure (VEC=7.33) ((**11**) in Fig. 1). However, attempts to form $CeFe_5$ at high pressure (25 kbar) and temperature (950 °C) failed.

3.3.2. $LaNi_4Mg$ and $NdNi_4Mg$

According to the maps these hypothetical compounds should crystallize with $CaCu_5$ type structures provided Mg is counted as a B element ((**12**)-$LaNi_4Mg$ and (**16**)-$NdNi_4Mg$ in Fig. 4). Compounds of that composition were indeed synthesised, but found to crystallize with the $MgCu_4Sn$ type structure, an ordered ternary derivative of $AuBe_5$. In this context it is worth recalling that the $AuBe_5$ structure is closely related to the $MgCu_2$ type structure (AB_2) in which magnesium can be considered as an A type rather than a B type component. This suggests that Mg containing compounds having $MgCu_4Sn$ type structures should be classified as AB_2 rather than AB_5 compounds which would explain their unexpected position in the AB_5 maps (see (**12b**)-$La_{0.5}Mg_{0.5}Ni_2$ and (**16b**)-$Nd_{0.5}Mg_{0.5}Ni_2$ in Fig. 4). This view is consistent with the fact that the La series $La_{1-x}Mg_xNi_2$ crystallizes with a disordered cubic $MgCu_2$ (C15) type structure at low Mg contents ($0<x<0.67$) and with the $MgNi_2$ (C36) type structure at higher Mg contents (x>0.67). As to the ordered compounds RNi_4Mg (R=La, Nd) they were found to absorb hydrogen reversibly in a useful range to compositions of up to RNi_4MgH_4 [14].

3.3.3. $LaNi_2Mn_3$

This hypothetical compound (R_A/R_B=1.466, VEC=7.33) is slightly outside the $CaCu_5$ type domain ((**9**) in Fig. 4) and inside the YNi_2Al_3 domain. Attempts to synthesize this compound were successful and its structure was found [15] to be of YNi_2Al_3 type. It is the first manganese member of this type. So far, only aluminium, gallium and tin members were known, and they were relatively poor hydrogen absorbers. Interestingly, $LaNi_2Mn_3$ displays excellent hydrogen storage properties and forms a reversible hydride of composition $LaNi_2Mn_3H_{4.6}$ [15].

3.3.4. YCu_3Al_2

This new compound [16] was reported after the present study was completed. It crystallizes with the $CaCu_5$ type structure and thus fits well onto the maps ((**5**) in Fig. 4).

4. Conclusions

The structural stability of AB_5 compounds has been modeled successfully based on atomic properties. Maps as

a function of R_A/R_B, $\Delta\chi$ and VEC reproduce well the stability domains of 15 structure types covering some 470 compounds. The maps have predictive power in the sense that they are capable of foreseeing structures of compounds that are thermodynamically stable. The successful synthesis of some new AB_5 compounds at 'predicted' compositions underlines the usefulness of the structure modeling approach for the search of new hydrogen storage materials.

Acknowledgements

This work has been supported by the Swiss National Science Foundation and the Swiss Federal Office of Energy.

References

[1] W.B. Pearson, Zeit. Kristallogr. 151 (1980) 301–315.
[2] K. Balkis Ameen, M.L. Bhatia, J. Alloys Comp. 347 (2002) 165–170.
[3] P. Villars, F. Hulliger, J. Less-Common Met. 132 (1987) 289–315.
[4] E. Teatum, K. Gschneider, J. Waber, LA-2345, US Department of Commerce, Washington, DC, 1960.
[5] A.I. Martynov, S.S. Batsanov, Russ. J. Inorg. Chem. 25 (12) (1980) 1737–1739.
[6] P. Villars, L.D. Calvert, in: Pearson's Handbook of Crystallographic Data for Intermetallic Phases, 2nd Ed, American Society for Metals, Materials Park, OH 44073, 1991.
[7] J.L.C. Daams, P. Villars, J.H.N. Van Vucht, in: Atlas of Crystal Structure Types for Intermetallic Phases, ASM International, Materials Park, OH 44073, 1991.
[8] Binary Alloy Phase Diagrams, ASM International, 2nd Edition, plus Updates (1996).
[9] P. Villars, A. Prince, H. Okamoto, in: Handbook of Ternary Alloy Phase Diagrams, ASM International, Materials Park, OH 44073, 1997.
[10] Red Books, Constitutional Data and Phase Diagrams of Metallic Systems 1990–1995, MSI, ASM International, Materials Park, OH 44073, 1998.
[11] L. Guénée, PhD-thesis No 3341, University of Geneva, 2002.
[12] K. Aono, S. Orimo, H. Fujii, J. Alloys Comp. 309 (2000) L1–L4.
[13] S. Pechev, J.-L. Bobet, B. Chevalier, B. Darriet, F. Weill, J. Solid State Chem. 150 (2000) 62–71.
[14] L. Guénée, V. Favre-Nicolin, K. Yvon, J. Alloys Comp. 348 (2003) 129–137.
[15] L. Guénée, K. Yvon, J. Alloys Comp. 348 (2003) 176–183.
[16] K. Kadir, T. Sakai, I. Uehara, L. Eriksson, Acta Crystallogr. C 57 (2001) 999–1000.